Journal of Magnetic Resonance 298 (2019) 23–30

Contents lists available at ScienceDirect

Journal of Magnetic Resonance

journal homepage: www.elsevier.com/locate/jmr

Broadband homodecoupled time-shared ^{1}H-^{13}C and ^{1}H-^{15}N HSQC experiments

Pau Nolis, Kumar Motiram-Corral, Míriam Pérez-Trujillo, Teodor Parella *

Servei de Ressonància Magnètica Nuclear, Universitat Autònoma de Barcelona, E-08193, Bellaterra, Barcelona, Catalonia, Spain

ARTICLE INFO

Article history:
Received 24 October 2018
Revised 19 November 2018
Accepted 20 November 2018
Available online 22 November 2018

Keywords:
NMR
Time-shared NMR
Pure-shift HSQC
HSQC
J-resolved HSQC
Proton-carbon coupling constants
Proton-nitrogen coupling constants

ABSTRACT

The concepts of pure-shift NMR and time-shared NMR are merged in a single experiment. A $^{13}C/^{15}N$ time-shared version of the real-time BIRD-based broadband homodecoupled HSQC experiment is described. This time-efficient approach affords simultaneously ^{1}H-^{13}C and ^{1}H-^{15}N pure-shift HSQC spectra in a single acquisition, while achieving substantial gains in both sensitivity and spectral resolution. We also present a related $^{13}C/^{15}N$-F2-coupled homodecoupled version of the CLIP-HSQC experiment for the simultaneous measurement of $^{1}J_{CH}$ and $^{1}J_{NH}$ from the simplified doublets observed along the direct dimension. Finally, a novel *J*-resolved HSQC experiment has been designed for the simple and automated determination of both $^{1}J_{CH}/^{1}J_{NH}$ from a 2D *J*-resolved spectrum.

1. Introduction

In the last years, the development of powerful broadband homodecoupling techniques and their implementation in a broad range of existing and novel experiments has emerged as a useful tool in modern small-molecule NMR spectroscopy [1]. This concept of pure-shift (ps) NMR affords a spectacular increase in spectral resolution because the typical wide *J* multiplet structures are simplified to singlets, minimizing signal overlap and making data analysis and interpretation much easier. Many different ps techniques are currently available, but we want to highlight two relevant contributions. The PSYCHE element [2] improves the sensitivity and performance of the original Zangger-Sterk experiment [3], allowing its successfully implementation in many interferogram-based 1D and 2D NMR experiments [4]. A second relevant contribution was the real-time broadband homodecoupling scheme based on BIRD (Bilinear Rotation Decoupling) elements [5,6] applied during ^{1}H acquisition in heteronuclear HSQC-type experiments [7,8]. The HSQC pulse train acts as a ^{1}H-^{13}C selection filter, and it is specifically designed to suppress the large ^{1}H-^{12}C contribution. In contrast to PSYCHE that is related to important sensitivity losses and longer acquisitions, the sensitivity and duration of the real-time pure-shift HSQC (psHSQC) is not affected when compared to the parent HSQC experiment. Recently, an excellent description on the practical aspects involved in real-time homodecoupled HSQC experiments has been reported. [9] For instance, the generation of artefacts or sidebands, the line broadening caused by transverse relaxation between data chunks and/or by the mismatch between BIRD timing and $^{1}J_{CH}$ values, or the effects of imperfect pulses are some of the issues to consider when implementing this technique.

Time-Shared (TS) NMR experiments allows the simultaneous acquisition of ^{1}H-^{13}C and ^{1}H-^{15}N spectra in spectrometers having a triple-channel hardware configuration [10,11]. These methods are particularly useful for molecules containing both carbon and nitrogen because two experiments that use the same pulse train can be concentrated in a single sequence. The performance of TS experiments relies in the fact that the evolution of ^{1}Hs attached to ^{13}C and ^{1}Hs attached to ^{15}N do not interference between them. These contributions can be successfully manipulated by designing pulse sequences that involve integrated $^{13}C/^{15}N$ pulses and shared delays to achieve similar effects in both nuclei at the same time. Several TS applications have been provided for the most common 2D heteronuclear experiments, such as CN-HSQC, CN-HSQC-TOCSY and CN-HMBC for small molecules [12–15], and also for multi-dimensional protein NMR [16–25]. The main advantage of the simultaneous TS acquisition compared to the conventional sequential acquisition of the two separate experiments is a considerable sensitivity-gain per time unit.

* Corresponding author.
E-mail address: teodor.parella@uab.cat (T. Parella).

https://doi.org/10.1016/j.jmr.2018.11.005
1090-7807/

In this article we show how the features offered by pure-shift NMR and time-shared NMR can be merged in a single NMR experiment. Thus, a $^{13}C/^{15}N$ time-shared version of the real-time BIRD-based broadband homodecoupled HSQC experiment is presented. This novel CN-psHSQC experiment affords simultaneously both pure-shift ^{1}H-^{13}C and ^{1}H-^{15}N HSQC spectra in a unique measurement, affording a substantial sensitivity gain per time unit when compared to the separate recording of each experiment. We also provide the $^{13}C/^{15}N$-F2-coupled homodecoupled version of the CLIP-HSQC experiment (CN-psCLIPHSQC) for the simultaneous measurement of $^{1}J_{CH}$ and $^{1}J_{NH}$ from the simplified doublets obtained along the direct dimension. We also show how other resolution-enhanced techniques, such as non-uniform sampling (NUS) or *J*-spectroscopy, can be incorporated into these experiments. Thus, a novel *J*-resolved HSQC experiment (referred to as CN-*J*-psHSQC) has been created for the easy and automated determination of both $^{1}J_{CH}/^{1}J_{NH}$ coupling values from the indirect dimension of a 2D *J*-resolved spectrum.

2. Results and discussion

The TS experiments proposed in this article use several criss-crossed NMR building blocks, such as mixed INEPT (CN-INEPT), BIRD^{d,X} (CN-BIRD^{d,X}), BIRD^{d} (CN-BIRD^{d}) and perfectBIRD (CN-perfectBIRD) elements (Fig. 1). Note that the number of carbon (nitrogen) pulses in these CN-based elements are the same found in the original single-nucleus ^{13}C (^{15}N) analogues. In terms of delays, the N-INEPT transfer ($\Delta_2 = 1/(4 * {}^{1}J_{NH}) = 2.78$ ms for 90 Hz) is longer than C-INEPT ($\Delta_1 = 1/(4*{}^{1}J_{CH}) = 1.85$ ms for 135 Hz) due to the lower magnitude of $^{1}J_{NH}$ vs $^{1}J_{CH}$. Thus, the CN-INEPT block which has the same duration than N-INEPT can generate some ^{13}C sensitivity loss by additional T_2 relaxation. This loss is bigger for the rest of CN-BIRD elements because delays are twice as long. However, ^{15}N is the limiting experiment in terms of sensitivity and therefore this expected ^{13}C signal loss becomes not critical. A detailed description of the main features of the basic BIRD^{d,X} and BIRD^{d} elements can be found in Refs. [5,6] and those of perfectBIRD in Refs. [30,34], and their effects on coupling constants and chemical shifts are summarized in Table S1.

The CN-psHSQC scheme depicted in Fig. 2 is derived from the original CN-HSQC experiment which already included CN-INEPT transfer elements and sensitive-enhancement PEP [26] to maximize signal intensities for both CH and NH spin systems. Basically, it is the pulse sequence shown in Fig. 1d of the reference [10] up to the detection period. Real-time BIRD-based homodecoupling is inserted during ^{1}H acquisition using the data chunk strategy described in the psHSQC experiment based on the G_7-180°(^{1}H)-G_7-G_8-CN-BIRD-G_8 cluster, where G_7 and G_8 stands for gradients plus their recovery delays. As a major novelty, we use the adapted CN-BIRD^{d} element introduced in Fig. 1C for the simultaneous homodecoupling of all detected ^{1}H-^{13}C and ^{1}H-^{15}N signals with respect to the passive ^{1}H-^{12}C and ^{1}H-^{14}N proton [8,9] instead of the BIRD^{d,X} element [7].

The resulting 2D CN-psHSQC spectrum shows all ^{1}H signals as singlets, except those from prochiral CH_2 and NH_2 groups that will show an additional splitting due to $^{2}J_{HH}$. The performance of this scheme has been tested on a standard sample of cyclosporine, a typical peptide containing all NH and CH_n (n = 1–3) multiplicities (Fig. 3). The relative positive/negative intensity of CH and NH cross-peaks in CN-psHSQC spectra results of the relative phase between the 90°(^{13}C) and 90°(^{15}N) pulses applied prior to the t_1 and $t_{1'}$ periods, respectively. By default, we apply $\phi_1 = x$ and $\phi_2 = -x$ to differentiate them as positive (CH) and negative (NH) cross-peaks. We have recorded a complete set of HSQC experiments under identical experimental and time conditions to analyze the experimental sensitivity ratios achieved per time unit: C-HSQC (4 scans per t_1 increment), N-HSQC (4 scans per t_1 increment), C-psHSQC (4 scans per t_1 increment), N-psHSQC (4 scans per t_1 increment), CN-HSQC (8 scans per t_1 increment) and CN-psHSQC (8 scans per t_1 increment). As already reported for the original CN-HSQC experiment, the simultaneous acquisition of ^{13}C and ^{15}N data by CN-psHSQC affords an averaged signal-to-noise (SNR) per time unit enhancement about 15–20% and 40% when compared to the individual C-psHSQC and N-psHSQC, respectively (Fig. 3B). This

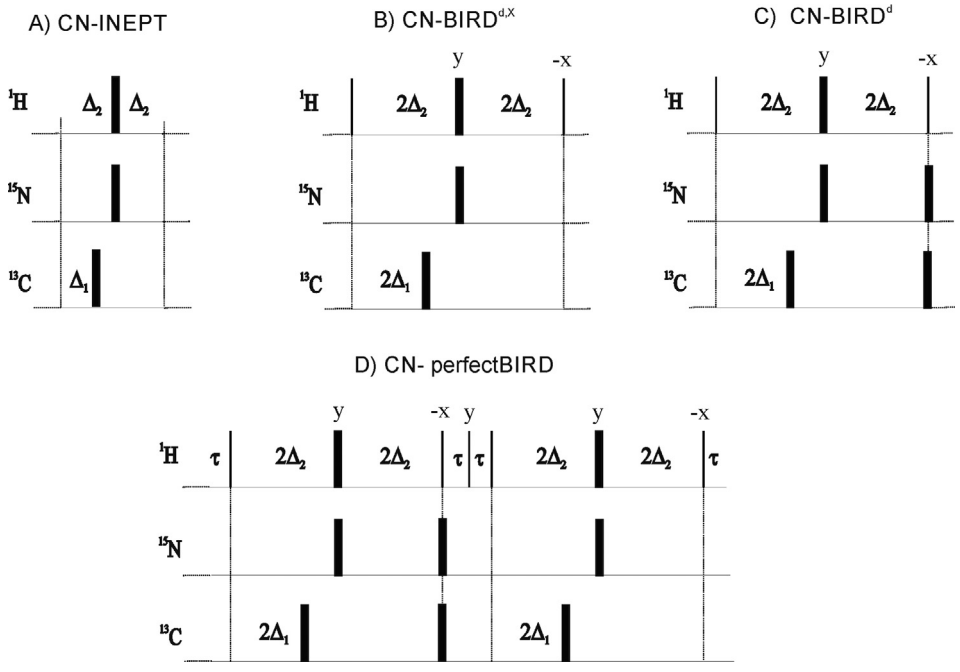

Fig. 1. Schematic representation of several NMR building blocks used in time-shared pure-shift NMR experiments: (A) CN-INEPT; (B) CN-BIRD^{d,X}; (C) CN-BIRD^{d} and (D) CN-perfectBIRD. Narrow and wide rectangular pulses refer to 90° and 180° pulses, respectively, along the x-axis unless indicated otherwise. The delays Δ_1 and Δ_2 are set to $1/(4^{*1}J_{CH})$ and $1/(4^{*1}J_{NH})$, respectively. 2τ is the echo period in the CN-perfectBIRD element.

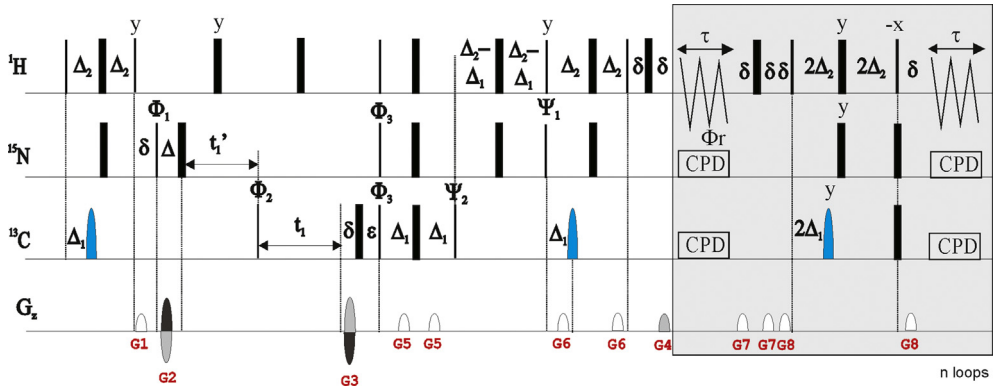

Fig. 2. Two-dimensional CN-psHSQC pulse sequence employing a pure-shift acquisition module using CN-BIRD^{d}. Narrow and wide rectangular pulses refer to 90° and 180° pulses, respectively, along the x-axis unless indicated otherwise. The inter-pulse delays are optimized according to $\Delta_1 = 1/(4^{*1}J_{CH})$ and $\Delta_2 = 1/(4^{*1}J_{NH})$, for maximizing CH and NH signals, respectively. The periods ε and Δ compensate evolution during the variable t_1 and t_1' periods and the time increments are set to $\Delta t_1 = 1/SW(^{13}C)$ and $\Delta t_1' = 1/SW$ (^{15}N)-1/SW(^{13}C). Phase cycle: $\phi_1 = (-x, x)$, $\phi_2 = (x, -x)$, $\phi_3 = (x, x, -x, -x)$, $\phi_r = (x, -x, -x, x)$. More information about gradients and other details can be found in the experimental section.

sensitivity gain can be reinforced by the signal collapsing achieved by homodecoupling which depends on the *J* coupling multiplet structure of each ^{1}H signal. Thus, whereas the intensities of singlets belonging to N-Me groups are obviously not enhanced by homodecoupling, substantial sensitivity enhancements up to 50–100% can be observed additionally for the more complex CH_α multiplets. On the other hand, the duration of the homodecoupling block (overall duration of the G_7-180°(^{1}H)-G_7-G_8-BIRD-G_8 cluster) is around 10.5 ms in C-psHSQC and 14.2 ms in N-psHSQC and CN-psHSQC experiments. This longer duration could introduce an additional line broadening factor caused by transverse relaxation between data chunks but, in practice, this effect is negligible for cyclosporine. In addition to all the advantages described above, CN-psHSQC dramatically improves the levels of spectral resolution, greatly avoiding signal overlap and expediting spectral analysis. Regarding spectrometer economy, all TS method also can take profit of the advantages of other resolution-enhanced methods, such as NUS, to increase the levels of F1 digital resolution per time unit or to speed up even more data acquisition. [27] Fig. S3 shows the practical implementation of 25% of NUS to improve the performance of CN-psHSQC, similarly as done in regular HSQC data, [28] obtaining both ^{13}C and ^{15}N data in shorter experimental times and/or improved digital resolution.

The measurement of $^{1}J_{CH}$ values from interferogram-based [29–31] and real-time [32] BIRD-based homodecoupled HSQC spectra has also received great interest for several research groups. As an extension of its applicability, the same pulse scheme of Fig. 2 can be slightly modified to obtain the F2-coupled CN-psHSQC spectrum, by omitting the broadband heteronuclear decoupling in both ^{13}C and ^{15}N channels during the FID acquisition and adding 90° ($^{13}C/^{15}N$) CLIP pulses prior to acquisition (Fig. S2). All ^{1}H signals in CN-psCLIPHSQC spectra appear as reduced doublet patterns from which the magnitude of both $^{1}J_{CH}$ and $^{1}J_{NH}$ can be easily determined along the F2 dimension (Fig. 4A). As discussed above, the major gains in resolution and sensitivity by signal multiplet collapsing are observed for CH cross-peaks. Besides, simplified peaks can expedite the measurement when accidental overlap occurs, as shown from H_α-4 and H_α-6 signals (Fig. 4B). As recently reported in Ref. [32], more accurate measurements could be performed cycling the radiofrequency pulses involved in the homodecoupling block both from chunk to chunk acquisition and from scan to scan during time averaging. These supercycle requirements lengthen the minimum phase cycle to be applied and therefore requires accumulating more scans per increment, increasing the acquisition time. It is also important to note that the real-time broadband homodecoupling technique fails to measure accurately $^{1}J_{CH}$ when strong coupling effects are present. One example is the strong coupling effects shown by the olefinic $H_{1\varepsilon}$ and $H_{1\zeta}$ protons resonating at 5.63 and 5.52 ppm, respectively ($^{3}J_{HH}$ = 15.5 Hz and separated by only 65 Hz). The two satellite components show a characteristic non-symmetrical pattern in all CLIPHSQC spectra that makes difficult a precise measurement of $^{1}J_{CH}$ in both conventional and homodecoupled signals (Fig. S4) [32].

The measurement of $^{1}J_{CH}$ from the indirect dimension of HSQC and *J*-resolved HSQC experiments has shown its utility for measuring scalar and residual dipolar couplings (RDCs) in small- and biomolecules. [33–38] Here we propose a novel time-shared *J*-resolved pure-shift HSQC (CN-*J*-psHSQC) experiment to perform the simultaneous measurement of $^{1}J_{CH}$ and $^{1}J_{NH}$ along the F1 dimension of a *J*-resolved spectrum (Fig. 5A). Data ^{1}H acquisition is performed using the mentioned real-time homodecoupling scheme based on the CN-BIRD^{d} cluster [8,9]. The major modifications are the replacement of the variable $^{13}C/^{15}N$ chemical shift t_1 and $t_{1'}$ evolution periods in the CN-psHSQC scheme by a fixed minimum period to allocate only the defocusing gradients, whereas the indirect dimension is generated by a *J*-coupling t_1 evolution period that substitutes the initial CN-INEPT transfer. As a basic implementation, a CN-BIRD^{d,X} element flanked by two purging gradients can be used as a central refocusing element in this t_1 period to avoid unwanted J_{HH} and long-range $^{n}J_{CH}$ and $^{n}J_{NH}$ contributions (Fig. S6A). However, $^{2}J_{HH}$ is modulated by both CN-BIRD^{d} and CN-BIRD^{d,X} clusters and therefore prochiral CH_2/NH_2 protons display doublets in both dimensions (Fig. S6B). We propose to use a CN-perfectBIRD as a refocusing element (Fig. 1D) to remove the $^{2}J_{HH}$ splitting in the F1 dimension. The CN-perfectBIRD consists of a longer $t_1/2$-CN-BIRD^{d}-$t_1/2$-$90_y(^{1}H)$-$t_1/2$-CN-BIRD^{d,X}-$t_1/2$ cluster [30,34] which can introduce some sensitivity penalty when short T_2 relaxation times are present but it works for all multiplicities (Fig. 5B). Because of the small SW(F1) used in the CN-*J*-psHSQC experiment (about 400–500 Hz), the incremented Δt_1 period becomes relatively long and therefore it is advisable to shorten the overall duration of the sequence to minimize deleterious T_2 effects. This is the main reason because the refocusing PEP scheme has been reduced to a shorter single echo CN-INEPT. It's worth mentioning that the homodecoupling properties of the perfectBIRD can be exploited only in the indirect dimension of a multidimensional experiment, as shown in Fig. 5A, [34] or in interferogram-based acquisition techniques, as reported in Ref. [30].

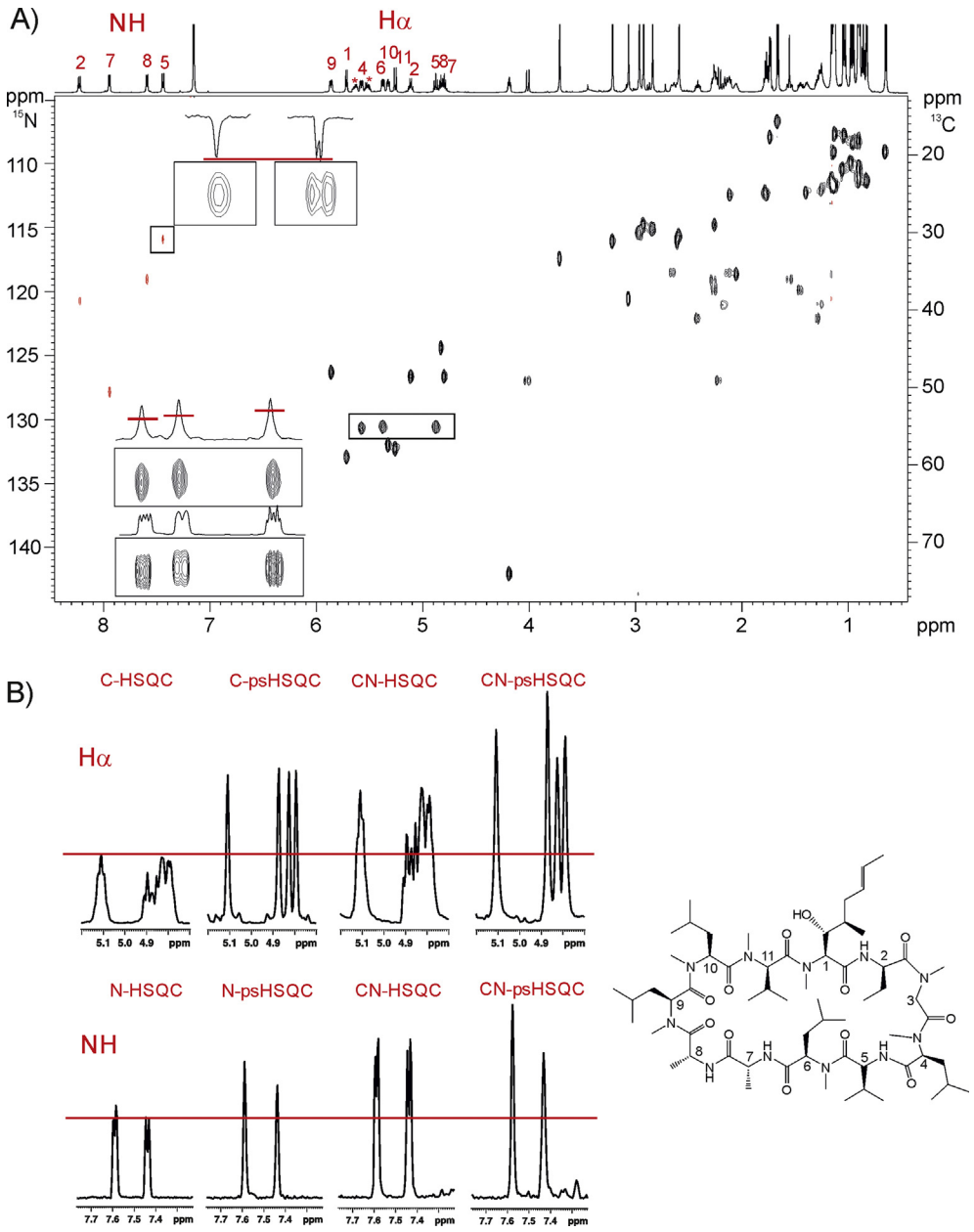

Fig. 3. (A) 2D CN-psHSQC spectrum of cyclosporine in benzene d_6. The expanded areas compare the relative sensitivity, multiplet simplification and linewidths obtained for some CH and NH cross-peaks using conventional and broadband homodecoupled ^{1}H acquisition. (B) Comparison of some CH and NH signal intensities and multiplet patterns obtained in C-HSQC (4 scans per t_1); N-HSQC(4 scans per t_1), C-psHSQC (4 scans per t_1); N-psHSQC(4 scans per t_1), CN-HSQC (8 scans per t_1) and CN-psHSQC (8 scans per t_1) experiments acquired in equivalent experimental times.

The benefits of the CN-*J*-psHSQC spectrum relay on its user-friendly *J*-resolved representation, yielding simplified singlets for both CH and NH signals along the detected dimension and clean symmetrical doublets due to $^1J_{CH}$ and $^1J_{NH}$ along the indirect dimension for all multiplicities (Fig. 4B). Signals in CN-*J*-psHSQC spectra show an antiphase coupling pattern along F1 which does not affect the easy $^1J_{CH}/^1J_{NH}$ measurement. The phases ϕ_1 and ϕ_2 determine the relative up-down (CH) or down-up (NH) phase of cross-peaks. Fig. 6 illustrates the advantages in terms of sensitivity-enhancement and spectral resolution achieved by broadband homodecoupling over the conventional acquisition mode in CN-*J*-psHSQC. The high resolution available in F1 (0.4 Hz/pt using 128 t_1 increments before data processing) allows the accurate extraction of $^1J_{CH}/^1J_{NH}$ for each cross-peak by only determining their y-axis coordinate. The excellent spectral sharpness affords valuable user-friendly $^1J_{CH}$ and $^1J_{NH}$ NMR profiles (Fig. 7), that identify each individual cross-peak and allows a rapid visualization of their coupling values for CHs (magnitudes around 135–142 Hz) and NHs (values around 92–94 Hz).

3. Conclusions

In summary, a set of time-shared pure-shift NMR experiments has been presented for the acquisition of homodecoupled ^{13}C and ^{15}N 2D HSQC spectra. Several CN-BIRD elements have been described for simultaneous ^{1}H-^{13}C and ^{1}H-^{15}N homodecoupling. It has been shown that the proposed experiments retain the known "sensitivity per time unit" benefits of the parallel TS acquisition of two different nuclei. Moreover, the full compatibility between sensitivity-enhanced PEP strategy and BIRD-based broadband

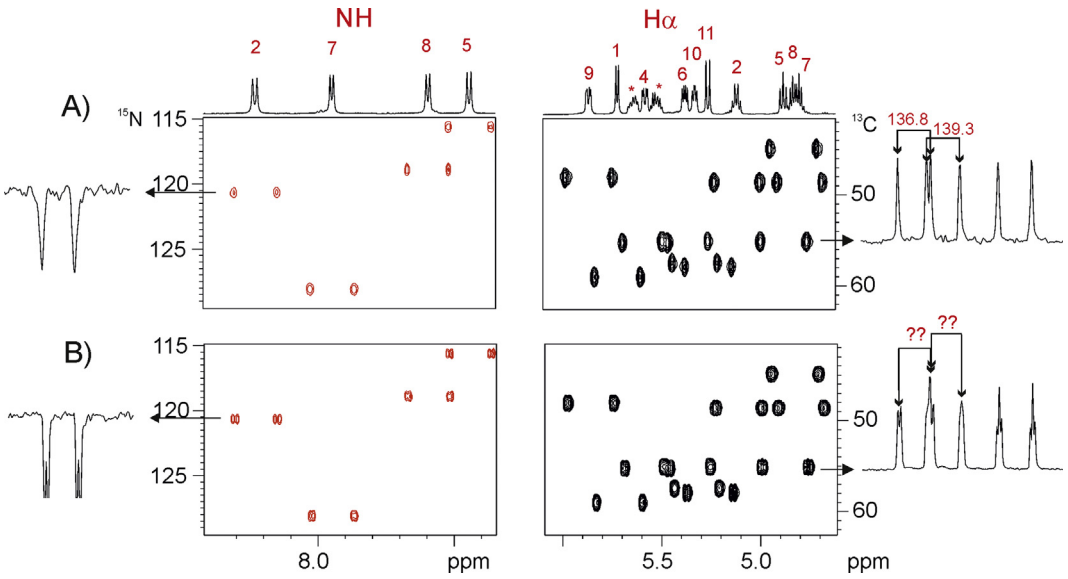

Fig. 4. Expansions corresponding to the (left) NH and (right) CH_α regions of the (A) CN-psCLIPHSQC and (B) CN-CLIPHSQC spectra of cyclosporine. 1D slices show specific rows in conventional and homodecoupled spectra.

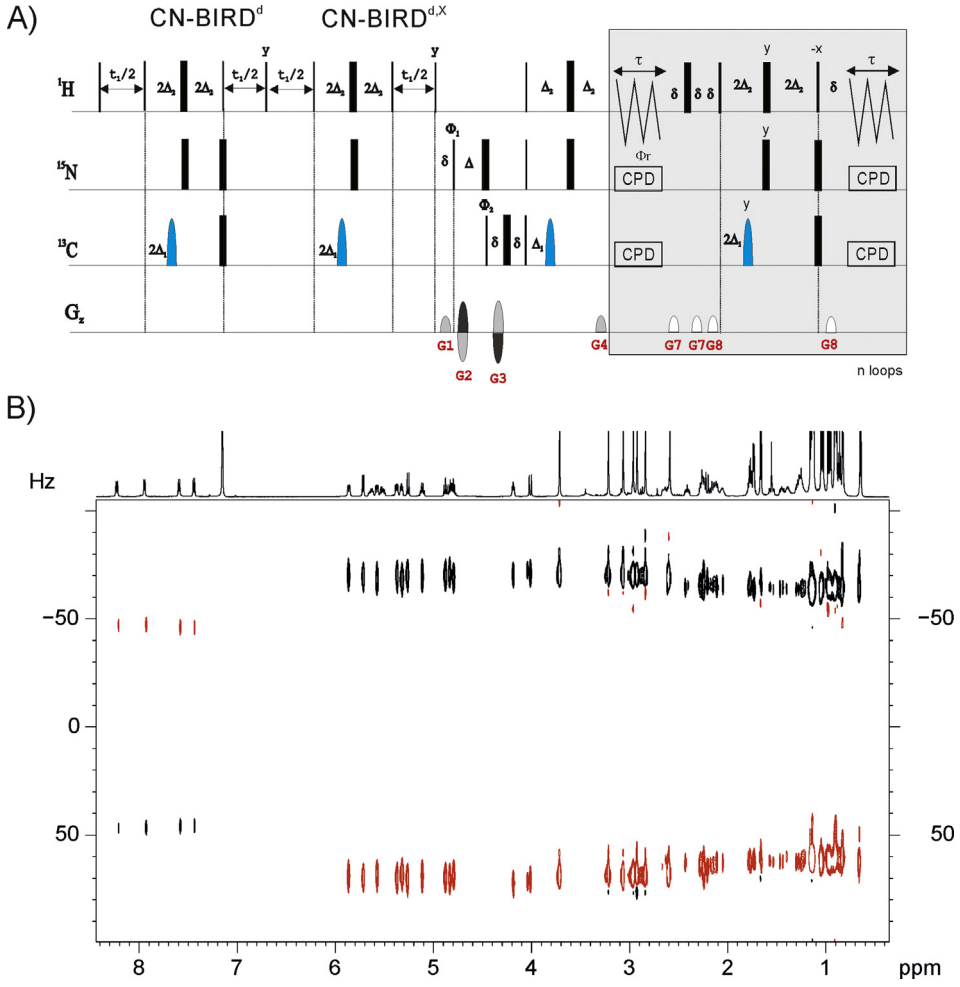

Fig. 5. (A) Pulse scheme of the CN-*J*-psHSQC experiment employing a CN-perfectBIRD element as a refocusing in t_1 and a pure-shift acquisition module using CN-BIRD^{d}. (B) 2D CN-*J*-psHSQC spectrum of cyclosporine, showing all NH (down-up multiplets) and CH (up-down multiplets) signals as clean doublet splittings along F1, irrespective of their multiplicities.

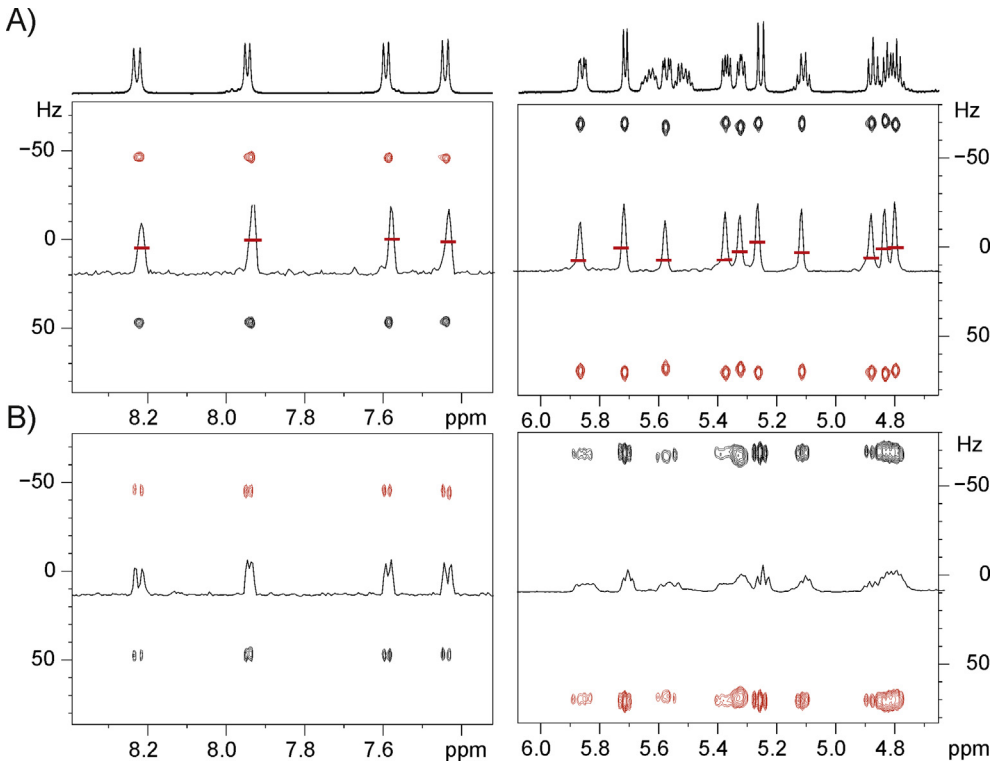

Fig. 6. Expansion of the NH and CHα region of the (A) CN-*J*-psHSQC and (B) CN-*J*-HSQC spectra. Both spectra have been acquired under identical parameters and overall experimental times. 1D internal projections are displayed for a real comparison about relative sensitivities and spectral resolution achieved in both experiments.

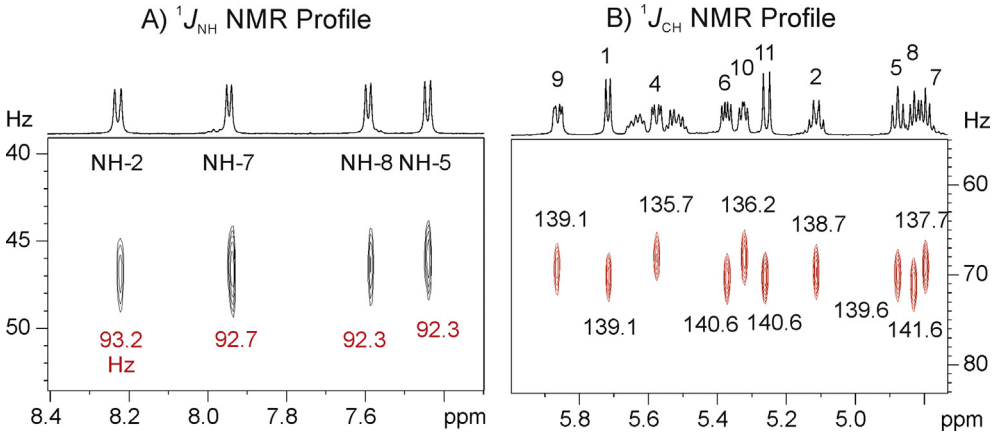

Fig. 7. Representative $^1J_{NH}$ and $^1J_{CH}$ NMR profiles of cyclosporine, displaying δ (^{1}H) in F2 and $^1J_{NH}/2$ and $^1J_{CH}/2$ in F1. The magnitude of the coupling constants can be extracted from the y coordinate of each cross-peak or using a simple phyton applet after conventional peak picking.

homodecoupling affords maximum levels of attainable sensitivity while spectral resolution is increased by *J* multiplet simplification. In practice, the longer evolution delays involved in the described concatenated NMR elements affects minimally to the ^{13}C signal intensities and linewidths. Two different methods to measure $^1J_{CH}$ and $^1J_{NH}$ simultaneously along the F1 or F2 dimension have been described. Of interest is the CN-*J*-psHSQC experiment that allows an accurate and automated determination of both $^1J_{CH}$ and $^1J_{NH}$ coupling values in a user-friendly *J*-resolved spectrum. This is an example showing how two resolution-enhanced techniques, such as pure-shift and *J*-resolved spectroscopy, can be efficiently combined with time-optimized time-sharing evolution in a single NMR experiment.

4. Experimental part

NMR experiments were recorded on a 600 MHz spectrometer equipped with a triple-resonance ^{1}H/^{13}C/^{15}N inverse probe. The sample used was 25 mM of cyclosporine dissolved in benzene d_6 and the temperature for all measurements was set to 300 K.

All spectra were recorded with proton 90° pulses of 8.3 μs and carbon 90° pulses of 21.5 μs. For broadband carbon inversion, 0.5 ms smoothed Chirp pulses sweeping over a frequency band of 60 kHz was used. ^{15}N heteronuclear decoupling was performed using GARP and ^{13}C heteronuclear decoupling using the adiabatic decoupling p5m4sp180.2 scheme. The ^{1}H, ^{13}C, ^{15}N carriers were centred at 5 ppm, 55 ppm and 120 ppm, respectively. For all exper-

iments, the duration of the pre-scan delay was 1s, the inter-pulse delays were optimized according to $\Delta_1 = 1/(4^*{}^1J_{CH}) = 1.85$ ms ($^1J_{CH} = 140$ Hz) and $\Delta_2 = 1/(4^*{}^1J_{NH}) = 2.78$ ms ($^1J_{NH} = 90$ Hz). Gradient ratios were set-up as percentage of the absolute gradient strength of 53.5 G/cm. All gradients had a rectangular shape with smoothed edges (SMSQ10.100 in Bruker nomenclature) and their durations (δ in ms) and strengths (%) were: G1 = (800 μs, 80), G2 = (1 ms, −47.63), G3 = (1 ms, 32.37), G4 = (1 ms, 8.14), G5 = (800 μs, 11.0), G6 = (800 μs, −5.0), G7 = (800 μs, 13.0), G8 = (800 μs, 17.0). Basic phase cycle: ϕ_1 = −x, x; ϕ_2 = x, −x; ϕ_3 = x, x, −x, −x; Ψ_1 = y, y, −y, −y; Ψ_2 = −y, −y, y, y; ϕ_r = x, −x, −x, x. All experiments were acquired and processed using the echo/anti-echo protocol where the echo and anti-echo signals were collected separately by inverting the sign of gradients G2 and G3 together with the inversion of Ψ_1 and Ψ_2. Real-time BIRD-based homodecoupling was performed using 14.97 ms chunk length (τ) and 6 loops, giving an acquisition time of 179 ms (2048 complex points in F2).

Experimental conditions of the CN-psHSQC experiments: 8 scans were accumulated for each one of the 128t_1 increments and the number of complex data points in t_2 was set to 2048. Prior to Fourier-transformation of each data, zero filling to 1024 in ω_1 and a π/2-shifted squared sine bell window function (QSINE, SSB: 2) in both dimensions were applied. The Δt_1 and $\Delta(t_1 + t_1')$ times were 23.7 μs and 189.3 μs, respectively, that correspond to spectral widths of 21128 Hz and 5283 Hz for ^{13}C and ^{15}N, respectively. The experimental conditions of the CN-psCLIPHSQC experiments were the same as described for the analog CN-psHSQC. We have not used the time-consuming chunk-to-chunk phase supercycle described in Ref. [32] because it lengthens the acquisition time very much. For accurate measurements, we strongly recommend the CN-*J*-psHSQC experiment.

Experimental conditions of the CN-*J*-psHSQC: 8 scans were accumulated for each one of the 128 t_1 increments and the number of complex data points in t_2 was set to 2048. Spectra were acquired with spectral widths of 5699 Hz (in F_2) and 500 Hz (in F_1), respectively. Prior to Fourier-transformation of each data, zero filling to 1024 in F1 and a π/2-shifted squared sine bell window function (QSINE, SSB: 2) in both dimensions were applied. After applying zero filling, the digital resolution was of 0.48 Hz in F1. An error of ± 0.5 Hz in the determination of $^1J_{CH}$ and $^1J_{NH}$ is assumed as a conservative estimate.

The java applet jmeasurement.jar described in the SI for extracting $^1J_{CH}$ automatically is available on request. Pulse programs are available in the supporting information.

Acknowledgments

Financial support for this research provided by Spanish MINECO (project CTQ2015-64436-P) is gratefully acknowledged. We also thank the Servei de Ressonància Magnètica Nuclear, Universitat Autònoma de Barcelona, for allocating instrument time to this project.

Appendix A. Supplementary material

Supplementary data associated with this article can be found, in the online version, at https://doi.org/10.1016/j.jmr.2018.11.005.

References

[1] L. Castañar, T. Parella, Broadband 1H homodecoupled NMR experiments: recent developments, methods and applications, Magn. Reson. Chem. 53 (2015) 399–426.
[2] M. Foroozandeh, R.W. Adams, N.J. Meharry, D. Jeannerat, M. Nilsson, G.A. Morris, Ultrahigh-resolution NMR spectroscopy, Angew. Chemie – Int. Ed. 53 (2014) 6990–6992.
[3] K. Zangger, H. Sterk, Homonuclear broadband-decoupled NMR spectra, J. Magn. Reson. 489 (1997) 486–489.
[4] M. Foroozandeh, R.W. Adams, M. Nilsson, G.A. Morris, Ultrahigh-resolution total correlation NMR spectroscopy, J. Am. Chem. Soc. 136 (2014) 11867–11869.
[5] J.P. Garbow, D.P. Weitekamp, A. Pines, Bilinear rotation decoupling of homonuclear scalar interactions, Chem. Phys. Lett. 93 (1982) 504–509.
[6] D. Uhrín, T. Liptaj, K.E. Kövér, Modified BIRD pulses and design of heteronueclear pulses sequences, J. Magn. Reson. 101 (1993) 41–46.
[7] L. Paudel, R.W. Adams, P. Király, J.A. Aguilar, M. Foroozandeh, M.J. Cliff, M. Nilsson, P. Sándor, J.P. Waltho, G.A. Morris, Simultaneously enhancing spectral resolution and sensitivity in heteronuclear correlation NMR spectroscopy, Angew. Chemie – Int. Ed. 52 (2013) 11616–11619.
[8] P. Király, R.W. Adams, L. Paudel, M. Foroozandeh, J.A. Aguilar, I. Timári, M.J. Cliff, M. Nilsson, P. Sándor, G. Batta, J.P. Waltho, K.E. Kövér, G.A. Morris, Real-time pure shift ^{15}N HSQC of proteins: a real improvement in resolution and sensitivity, J. Biomol. NMR. 62 (2015) 43–52.
[9] P. Király, M. Nilsson, G.A. Morris, Practical aspects of real-time pure shift HSQC experiments, Magn. Reson. Chem. 56 (2018) 993–1005.
[10] M. Sattler, M. Maurer, J. Schleucher, C. Griesinger, A simultaneous 15N,1H- and 13C,1H-HSQC with sensitivity enhancement and a heteronuclear gradient echo, J. Biomol. NMR 5 (1995) 97–102.
[11] T. Parella, P. Nolis, Time-shared NMR experiments, Concepts Magn. Reson. Part A Bridg. Educ. Res. 36 (2010) 1–23.
[12] M. Pérez-Trujillo, P. Nolis, W. Bermel, T. Parella, Optimizing sensitivity and resolution in time-shared NMR experiments, Magn. Reson. Chem. 45 (2007) 325–329.
[13] P. Nolis, T. Parella, Simultaneous α/β spin-state selection for ^{13}C and ^{15}N from a time-shared HSQC-IPAP experiment, J. Biomol. NMR 37 (2007) 65–77.
[14] P. Nolis, M. Pérez-Trujillo, T. Parella, Multiple FID acquisition of complementary HMBC data, Angew. Chem. Int. Ed. Engl. 46 (2007) 7495–7497.
[15] Nolis P, Pérez-Trujillo M, Parella T. Time-sharing evolution and sensitivity enhancements in 2D HSQC-TOCSY and HSQMBC experiments, 44 (2006) 1031–1036.
[16] D.A. Snyder, Y. Xu, D. Yang, R. Brüschweiler, Resolution-enhanced 4D 15N/13C NOESY protein NMR spectroscopy by application of the covariance transform, J. Am. Chem. Soc. 129 (2007) 14126–14127.
[17] D.P. Frueh, H. Arthanari, G. Wagner, Unambiguous assignment of NMR protein backbone signals with a time-shared triple-resonance experiment, J. Biomol. NMR 33 (2005) 187–196.
[18] D.P. Frueh, D.A. Vosburg, C.T. Walsh, G. Wagner, Determination of all nOes in1H-13C-Me-ILV-U-2H-15N proteins with two time-shared experiments, J. Biomol. NMR 34 (2006) 31–40.
[19] P. Würtz, O. Aitio, M. Hellman, P. Permi, Simultaneous detection of amide and methyl correlations using a time shared NMR experiment: application to binding epitope mapping, J. Biomol. NMR 39 (2007) 97–105.
[20] S.H. Mishra, B.J. Harden, D.P. Frueh, A 3D time-shared NOESY experiment designed to provide optimal resolution for accurate assignment of NMR distance restraints in large proteins, J. Biomol. NMR 60 (2014) 265–274.
[21] M. Burgering, R. Boelens, R. Kaptein, Observation of intersubunit NOEs in a dimeric P22 Mnt repressor mutant by a time-shared [15N, 13C] double half-filter technique, J. Biomol. NMR 3 (1993) 709–714.
[22] R. Boelens, M. Burgering, R.H. Fogh, R. Kaptein, Time-saving methods for heteronuclear multidimensional NMR of (13C,15N) doubly labeled proteins, J. Biomol. NMR 4 (1994) 201–213.
[23] L.E. Kay, M. Wittekind, M.A. McCoy, M.S. Friedrichs, L. Mueller, 4D NMR triple-resonance experiments for assignment of protein backbone nuclei using shared constant-time evolution periods, J. Magn. Reson. 98 (1992) 443–450.
[24] Y. Xu, D. Long, D. Yang, Rapid data collection for protein structure determination by NMR spectroscopy, J. Am. Chem. Soc. 129 (2007) 7722–7723.
[25] C. Guo, D. Zhang, V. Tugarinov, An NMR experiment for simultaneous TROSY-based detection of amide and methyl groups in large proteins, J. Am. Chem. Soc. 130 (2008) 10872–10873.
[26] L.E. Kay, P. Keifer, T. Saarinen, Pure absorption gradient enhanced heteronuclear single quantum correlation spectroscopy with improved sensitivity, J. Am. Chem. Soc. 114 (1992) 10663–10665.
[27] S.G. Hyberts, H. Arthanari, G. Wagner, Applications of non-uniform sampling and processing, Top. Curr. Chem. 316 (2012) 125–148.
[28] A. Le Guennec, J.-N. Dumez, P. Giraudeau, S. Caldarelli, Resolution-enhanced 2D NMR of complex mixtures by non-uniform sampling, Magn. Reson. Chem. 53 (2015) 913–920.
[29] I. Timári, L. Kaltschnee, A. Kolmer, R.W. Adams, M. Nilsson, C.M. Thiele, G.A. Morris, K.E. Kövér, Accurate determination of one-bond heteronuclear coupling constants with "pure shift" broadband proton-decoupled CLIP/CLAP-HSQC experiments, J. Magn. Reson. 239 (2014) 130–138.
[30] L. Kaltschnee, A. Kolmer, I. Timári, V. Schmidts, R.W. Adams, M. Nilsson, K.E. Köver, G.A. Morris, C.M. Thiele, "Perfecting" pure shift HSQC: full homodecoupling for accurate and precise determination of heteronuclear couplings, Chem. Commun. 50 (2014) 15702–15705.
[31] T. Reinsperger, B. Luy, Homonuclear BIRD-decoupled spectra for measuring one-bond couplings with highest resolution: CLIP/CLAP-RESET and constant-time-CLIP/CLAP-RESET, J. Magn. Reson. 239 (2014) 110–120.
[32] I. Timári, L. Kaltschnee, M.H. Raics, F. Roth, N.G.A. Bell, R.W. Adams, M. Nilsson, D. Uhrín, G.A. Morris, C.M. Thiele, K.E. Kövér, Real-time broadband proton-homodecoupled CLIP/CLAP-HSQC for automated measurement of heteronuclear one-bond coupling constants, RSC Adv. 6 (2016) 87848–87855.

[33] T. Parella, Current developments in homonuclear and heteronuclear *J* -resolved NMR experiments, Magn. Reson. Chem. 56 (2018) 230–250.
[34] N. Marcó, A.A.A. Souza, P. Nolis, R.R. Gil, T. Parella, Perfect ^{1}JCH-resolved HSQC: Efficient measurement of one-bond proton-carbon coupling constants along the indirect dimension, J. Magn. Reson. 276 (2017) 37–42.
[35] L. Castañar, M. Garcia, E. Hellemann, P. Nolis, R.R. Gil, T. Parella, One-shot determination of residual dipolar couplings: application to the structural discrimination of small molecules containing multiple stereocenters, J. Org. Chem. 81 (2016) 11126–11131.
[36] B. Luy, J.P. Marino, JE-TROSY: combined J- and TROSY-spectroscopy for the measurement of one-bond couplings in macromolecules, J. Magn. Reson. 163 (2003) 92–98.
[37] J. Furrer, M. John, H. Kessler, B. Luy, J-Spectroscopy in the presence of residual dipolar couplings: determination of one-bond coupling constants and scalable resolution, J. Biomol. NMR 37 (2007) 231–243.
[38] J.D. Snider, E. Troche-Pesqueira, S.R. Woodruff, C. Gayathri, N.V. Tsarevsky, R.R. Gil, New strategy for RDC-assisted diastereotopic proton assignment using a combination of J-scaled BIRD HSQC and J-scaled BIRD HMQC/HSQC, Magn. Reson. Chem. 50 (2012) S86–S91.